HHS Public Access

Author manuscript

AJR Am J Roentgenol. Author manuscript; available in PMC 2020 October 17.

Published in final edited form as:

AJR Am J Roentgenol. 2019 June ; 212(6): 1234–1243. doi:10.2214/AJR.19.21172.

Role of Virtual Biopsy in the Management of Renal Masses

Alberto Diaz de Leon[1], **Matthew S. Davenport**[2], **Stuart G. Silverman**[3], **Nicola Schieda**[4], **Jeffrey A. Cadeddu**[1,5], **Ivan Pedrosa**[1,5,6]

[1]Department of Radiology, University of Texas Southwestern Medical Center, 2201 Inwood Rd, Ste 210, Dallas, TX 75225.

[2]Departments of Radiology and Urology, Michigan Medicine, Ann Arbor, MI.

[3]Department of Radiology, Brigham and Women's Hospital, Boston, MA.

[4]Department of Medical Imaging, University of Ottawa, Ottawa Hospital, Ottawa, ON, Canada.

[5]Department of Urology, University of Texas Southwestern Medical Center, Dallas, TX.

[6]Advanced Imaging Research Center, University of Texas Southwestern Medical Center, Dallas, TX.

Abstract

OBJECTIVE.—Renal masses comprise a heterogeneous group of pathological conditions, including benign and indolent diseases and aggressive malignancies, complicating management. In this article, we explore the emerging role of imaging to provide a comprehensive noninvasive characterization of a renal mass—so-called "virtual biopsy"—and its potential use in the management of patients with renal tumors.

CONCLUSION.—Percutaneous renal mass biopsy (RMB) remains a valuable method to provide a presurgical histopathologic diagnosis of renal masses, but it is an invasive procedure and is not always feasible. Accumulating data support the use of imaging features to predict histopathology of renal masses. Imaging may help address some of the inherent limitations of RMB, and in certain settings, a multimodal clinical approach may allow decreasing the need for RMB.

Keywords

CT; MRI; renal cell carcinoma; renal mass; renal mass biopsy

In the United States, there has been a steady increase in the incidence of kidney cancer, estimated at 65,430 cases in 2018 [1], that is thought to be largely the result of the burgeoning use of cross-sectional imaging and the incidental detection of renal masses. However, despite an overall aggressive approach in treating these masses, kidney cancer mortality has not declined [2–4]. As a result, radiologists and urologists are challenged with distinguishing benign from malignant renal masses and determining which cancers are best managed with active surveillance (AS), all to avoid overtreatment of benign masses and those cancers that are unlikely to affect a patient's health.

Address correspondence to I. Pedrosa (ivan.pedrosa@utsouthwestern.edu).

I. Pedrosa is on the scientific advisory board of Bayer Healthcare.

Kidney cancer is most commonly diagnosed as an incidental small (≤ 4 cm) renal mass [2]. However, a substantial number of renal masses of this size are benign (e.g., fat-poor angiomyolipoma [AML], oncocytoma) [3] and may appear similar to renal cell carcinoma (RCC). The prevalence of benign disease is indirectly correlated with mass size [3]. Benign pathology is found in approximately 40% of resected renal masses less than 1 cm and in approximately 20% of masses between 1 and 4 cm [4]. The increased incidence of incidental renal masses has been associated with an 82% increase in the number of surgical resections for benign tumors between 2000 and 2009 in the United States [4].

RCCs are subdivided in the World Health Organization classification into different histologic subtypes [5]. The most common subtypes include clear cell RCC (ccRCC), which accounts for 70–75% of all RCCs, followed by papillary RCC (pRCC; 10–21%) and chromophobe RCC (chrRCC; 5%) [5, 6]. Patient survival depends on a variety of factors, including tumor stage, histologic subtype, histologic grade (i.e., International Society of Urological Pathology [ISUP] grade), presence of sarcomatoid features, and necrosis. An increased frequency of high-grade disease in RCC (i.e., ISUP grades 3 and 4) has been documented with increasing tumor size [7, 8]. Specifically, the reported prevalence of high-grade tumors is 0% up to 2 cm, 17% between 2 and 4 cm, and approximately 40% when larger than 4 cm [8]. Furthermore, ccRCC is associated with a worse prognosis than pRCC and chrRCC in patients with similar tumor stage [5, 9].

The American Urological Association guidelines for management of renal masses considers AS as a potential option for select patients with T1a (≤ 4 cm) or T1b (> 4 and ≤ 7 cm) RCC, particularly those with comorbidities or limited life expectancy [10]. However, AS approaches are currently applied primarily to patients with cT1a disease. This is likely because of the perceived increased risk of progression during AS in patients with more advanced stage disease, despite the reported low risk of metastases in T1b tumors [11]. The lack of reliable predictors of oncologic behavior and the potential limitation of tissue sampling to adequately predict histologic subtype and grade in larger heterogeneous tumors likely limit the applicability of AS in clinical practice for patients with T1b disease. In addition to informing AS strategies, an accurate presurgical histologic diagnosis is critical for neoadjuvant protocols in patients with localized and locally advanced disease, many of whom present with heterogeneous masses. Therefore, there is also an opportunity to apply imaging methods for improved characterization of renal masses in these clinical scenarios.

Although percutaneous renal mass biopsy (RMB) is useful today, it typically samples a tumor in one location. A noninvasive method that characterizes renal masses and provides a virtual assessment of an entire potentially heterogeneous tumor could help direct management by determining which patients may or may not be safely considered for AS or may benefit from additional evaluation. Similarly, a noninvasive presurgical evaluation of the entire tumor may complement RMB and assist in the implementation of neoadjuvant therapy protocols. In this article, we explore the emerging role of imaging to provide a comprehensive noninvasive characterization of a renal mass—so-called “virtual biopsy”—and its potential use in the management of patients with renal tumors.

Need for an Image-Based Virtual Biopsy: Limitations of Percutaneous Biopsy

RMB is a valuable method that can provide a presurgical histopathologic diagnosis of solid renal masses in many patients. It can be used to guide clinical decisions and treatment strategies and to help diagnose hematologic, metastatic, infectious, and inflammatory causes [10, 12]. RMB is also the only way to obtain a definitive histopathologic diagnosis before percutaneous ablation and can help guide management after treatment. Perhaps its most important role is in the diagnosis of benign tumors so that patients with these lesions do not undergo unnecessary resection or ablation. Indeed, a statistically significant decrease in the surgical resection of benign disease has been reported when RMB is performed routinely for T1a disease [13]. However, RMB is not indicated when it is unlikely to affect management recommendations or patient preferences (e.g., severe medical comorbidities prohibiting treatment); such a patient would likely be managed conservatively regardless of histopathology results. Biopsy or aspiration of cystic masses is controversial because of the potential for tumor spillage and the high likelihood of obtaining a nondiagnostic result. In general, RMB of solid masses is well tolerated with a low rate of reported complications.

Although RMB is now largely accepted in clinical practice [10, 14–16], there are several limitations of RMB that an imaging-based virtual biopsy would address. First, biopsy is an invasive test. The most common complication is hemorrhage, but the incidence of hemorrhage requiring intervention is less than 1% [17,18] (Fig. 1). The risk of needle track tumor seeding is rare, with one systematic review of 2979 patients and 3113 RMBs reporting only a single case [18]. Clinically significant pain (1.2%), gross hematuria (1.0%), and pneumothorax (0.6%) are other less common complications [18]. An additional and potentially underrecognized risk is pathologic upstaging. An analysis of 24,548 patients with cT1a renal masses in the National Cancer Database from 2010 to 2013 found a 1% increased likelihood of upstaging from cT1a to pT3a (i.e., involvement of perirenal fat) in patients with RCC undergoing RMB [19].

Second, the results of percutaneous RMB may not be definitive, particularly when the results show no malignant cells and a specific benign diagnosis is not rendered. A systematic review conducted by Patel et al. [18] reported a pooled sensitivity of 97.5%, specificity of 96.2%, and positive predictive value (PPV) of 99.8% for RMB. However, the frequency of nondiagnostic sampling was 14% and the negative predictive value (NPV) was only 63%, indicating that 37% of patients were ultimately found to have malignant disease at time of surgical resection despite an initial negative biopsy. Importantly, most reports addressing the diagnostic accuracy of RMB include only those masses for which the biopsy was attempted; inclusion of patients in whom RMB is considered technically too difficult or unsafe and therefore is not pursued would invariably result in a lower diagnostic performance.

Third, perhaps because of the heterogeneity of certain tumors, the reported accuracy of RMB for tumor grade has been highly variable, ranging between 52% and 76%, with 16% of tumors upgraded from low-grade to high-grade on final surgical pathology [18]. The latter is particularly relevant in patients with small renal masses being considered for AS because tissue biopsies represent only a small portion of the tumor. Additionally, the accuracy of

RMB in diagnosing oncocytomas is limited. A 2017 systematic review of 205 oncocytic neoplasms identified by RMB, of which 46 underwent resection, found a PPV of 67% [20].

Finally, RMB adds cost and is billed separately from the imaging test that was used to characterize a renal mass. The costs of sedation and image guidance, as well as the procedure, are important considerations for diagnostic algorithms that attempt to incorporate RMB for a large proportion of solid masses.

Imaging Characterization of Renal Masses: The Virtual Biopsy

The noninvasive characterization of renal masses with imaging has several advantages. First, in many cases, it can be performed “for free” during the renal mass protocol imaging test that is used for characterization. There is no additional cost to the patient, no added direct procedure-related risk, and no subsequent appointment for additional testing. Second, it can be used to evaluate an entire tumor, not just a small sample as with RMB. This capability is especially important in characterizing heterogeneous tumors. Third, imaging can be repeated at multiple time points (e.g., during AS) and can be used to detect changes in mass features that may reflect alterations in tumor histology and aggressiveness. It would be impractical to repeat an RMB at multiple surveillance time points. Fourth, a noninvasive evaluation with imaging is possible in virtually every patient, whereas RMB is sometimes technically too difficult or unsafe.

CT

Tumor enhancement characteristics at CT may be used to suggest renal mass histology, with several general patterns described. Clear cell RCC is most often hypervascular with a degree of enhancement equal to or more than the renal cortex during the corticomedullary phase (acquired 40–70 seconds after contrast material injection) [21–23]. In contrast, pRCC almost always enhances less than the renal cortex during the corticomedullary phase and shows peak enhancement during the nephrographic phase (100–120 seconds after contrast material injection) [21–23]. In some cases, pRCC may not reach attenuation thresholds diagnostic for enhancement (e.g., ≥ 20 HU) depending on the timing of contrast-enhanced imaging [21, 24, 25].

Qualitatively distinguishing oncocytoma from ccRCC is challenging at CT because both often avidly enhance during the corticomedullary phase [22, 26]. However, other features have been suggested to aid in differentiation. The presence of segmental enhancement inversion (SEI)—defined as containing both avidly enhancing and hypoenhancing segments on the corticomedullary phase that reverse on the nephrographic phase—was initially reported to favor oncocytoma [27]. However, SEI is a controversial imaging finding that has been disputed by several groups and suffers from a lack of reproducibility and low interobserver agreement [28].

A quantitative assessment of attenuation values may add value. Herts et al. [25] found that using a tumor-to-aorta ratio of less than 0.25 and a tumor-to-parenchyma ratio of less than 0.25 resulted in NPVs of 98% and 95%, respectively, for the diagnosis of pRCC. Young et al. [21] used multiphasic threshold levels of 106 HU in the corticomedullary phase (40–55

seconds), 92 HU in the nephrographic phase (90–120 seconds), and 68 HU in the excretory phase (≈ 8 minutes) to achieve 77% accuracy, 86% sensitivity, and 85% PPV to differentiate ccRCC from oncocytoma. To distinguish ccRCC from pRCC, an accuracy of 85% was achieved using multiphasic threshold levels of 55 HU in the corticomedullary phase, 65 HU in the nephrographic phase, and 55 HU in the excretory phase [21]. Similarly, multiphasic threshold levels of 75 HU in the corticomedullary phase, 85 HU in the nephrographic phase, and 60 HU in the excretory phase were reported to have an accuracy of 85% in discriminating ccRCC from chrRCC [21]. These data indicate that contrast-enhanced CT can be used to inform the histologic subtype of a solid renal mass. However, CT accuracy is not perfect, the available data are mostly retrospective, and a CT-based virtual biopsy generally requires obtaining numerous contrast-enhanced phases that increase the radiation burden to the patient.

Distinction of fat-poor AML and RCC with CT is challenging. Like ccRCC, these benign tumors usually avidly enhance in the corticomedullary phase [29, 30]. However, fat-poor AML is most often small (≤ 3 cm), is hyperattenuating relative to renal parenchyma, enhances homogeneously, and appears to wash out in delayed contrast-enhanced phases [30, 31]. Kim et al. [29] used an absolute washout ratio of 13.4 to discriminate fat-poor AML from ccRCC and reported a sensitivity of 85%, specificity of 84.2%, PPV of 85.5%, NPV of 80%, and accuracy of 85%. The absolute washout ratio they studied was calculated by subtracting the attenuation on corticomedullary phase from excretory phase attenuation and then dividing by the change in attenuation between corticomedullary phase and unenhanced images.

Texture analysis, a technique that assesses heterogeneity of pixel intensities and gray-level values in a specific ROI, has been explored at CT to aid in differentiation and classification of renal masses. Preliminary experience indicated that entropy (a measure of histogram uniformity) and SD were useful in the distinction of ccRCC and non-ccRCC tumors on whole-lesion analyses at portal venous phase imaging [32]. Global heterogeneity features also have been reported to be significantly greater for sarcomatoid RCC [33]. A 2015 retrospective study of 16 fat-poor AMLs and 84 RCCs reported accurate differentiation of fat-poor AML from RCC using CT texture analysis at unenhanced CT, but that study did not have a validation cohort to confirm the texture thresholds reported [34].

Artificial intelligence and machine learning algorithms also have been preliminarily applied to differentiate histologic subtypes of renal masses with CT. One pilot study used random forest classification, a method that classifies samples into known classes using a hierarchy of variables, to generate and apply a model to 19 renal lesions consisting of oncocytomas, simple cysts, ccRCCs, and pRCCs. Using data generated from arterial, nephrographic, and excretory phase images, the model correctly classified all 19 lesions [35]. The combination of machine learning and texture features showed promising results in a pilot study of 58 patients including 17 fat-poor AMLs [36]. In that study, the accuracy, sensitivity, specificity, and AUC for differentiating fat-poor AML from RCC were 93.9%, 87.8%, 100%, and 0.95, respectively [36]. However, in each of these studies, the number of included masses was very small [35, 36]. Use of machine learning algorithms generally requires a much larger dataset to avoid statistical overfitting.

Although the application of texture analysis and machine learning to subtype renal masses at CT is currently an area of intense research, as of 2018, its use is considered preliminary and unverified.

MRI

The utility of multiparametric MRI (mpMRI) in the evaluation of renal masses has been well described [37–42]. The knowledge of enhancement patterns reported with CT can be applied to mpMRI because both iodinated contrast media and gadolinium-based contrast media exhibit similar extracellular properties. However, mpMRI offers information about many more tissue properties than CT that can be exploited for the characterization of renal masses and has the advantage of multiple dynamic phases without the penalty of cumulative ionizing radiation.

The use of sequences such as T2-weighted and dual-echo gradient-echo T1-weighted imaging together with contrast-enhanced imaging is commonly described as mpMRI and has been applied to the characterization of renal masses [43, 44]. Although the role of DWI is still under evaluation, this sequence is frequently reported as part of mpMRI protocols [44].

Clear cell RCC more often shows hyperintense signal on T2-weighted images relative to renal cortex and avid enhancement (205% enhancement) during the corticomedullary phase (timed to the arterial phase with a test bolus) [37, 45, 46]. Intratumoral areas of hypointense signal on shorter-TE opposed-phase images relative to longer-TE in-phase images are secondary to intracytoplasmic microscopic fat and are present in many ccRCCs [46–48]. In contrast, pRCC most often appears hypointense on T2-weighted images relative to renal cortex and exhibits mild enhancement during the corticomedullary phase (32% enhancement), which increases progressively on later phases [37, 47] (Fig. 2). Papillary RCC may be isointense to renal cortex or show hyperintense signal on unenhanced T1-weighted images, the latter of which is thought to be secondary to intralesional hemorrhage. Oncocytoma and chrRCC can show variable patterns of signal intensity and enhancement. Most commonly, oncocytomas exhibit a degree of enhancement comparable to that of ccRCC, whereas chrRCC tends to enhance to a level between ccRCC and pRCC (110% enhancement) [37]. In our experience, the eosinophilic variant of chrRCC constitutes an exception, with at least some of these tumors showing intense enhancement during the corticomedullary phase. The enhancement levels observed in ccRCC, pRCC, and chrRCC result in a tumor-to-cortex enhancement ratio of 1.4, 0.2, and 0.6, respectively, using images obtained during the corticomedullary phase [37].

As with CT, SEI also can be identified at mpMRI and used to suggest the diagnosis of oncocytoma [40, 49]. Kay et al. [40] found that the presence of SEI at mpMRI was an independent predictor for the diagnosis of oncocytoma (odds ratio = 16.21; 95% CI, 1.0–275.4), but the CI was wide (approaching 1) and the interobserver agreement was only moderate(κ = 0.49). Rosenkrantz et al. [49] reported SEI in both oncocytomas and chrRCCs, making the distinction between these two subtypes based on this imaging finding alone not reliable.

Fat-poor AML is usually homogeneous and is almost always hypointense on T2-weighted images relative to renal cortex [46, 47, 50]. The hypointensity on T2-weighted imaging also is common with pRCC, but some differences exist that help in differentiation. Fat-poor AML commonly exhibits intense enhancement during the corticomedullary phase, whereas pRCC has slow progressive enhancement, and pRCC is more likely than fat-poor AML to be heterogeneous. Compared with ccRCC, fat-poor AML shows a greater change in signal intensity from arterial to delayed phase images [50]. This change in signal intensity can be quantified using the arterial-delayed enhancement ratio reported by Sasiwimonphan et al. [50]. In their study, the arterial-delayed enhancement ratio was calculated by obtaining the difference between signal intensity in the arterial phase images (time of acquisition in that study was determined by adding the contrast material arrival time to the aorta to half the time of contrast material injection duration, subtracted by half the time of image acquisition plus 3 seconds) and unenhanced images, and dividing that difference by the difference in signal intensity on delayed phase (3 minutes after contrast injection) and unenhanced images. An arterial-delayed enhancement ratio of greater than 1.5 is more frequently seen with fat-poor AML than ccRCC. The combination of a T2 ratio of less than 0.9 (i.e., defined in the same study as the signal intensity of the tumor relative to renal cortex on T2-weighted images) and an arterial-delayed enhancement ratio of greater than 1.5 has a sensitivity and specificity of 70% and 99%, respectively, for differentiation of fat-poor AML from RCC (Fig. 3). Although this reported sensitivity may be low, a high specificity is arguably more desirable in the diagnosis of fat-poor AML because, other than the rare epithelioid variant, it is a tumor that does not warrant treatment.

DWI has been explored for the characterization of renal masses. Overall, benign renal masses have been reported to show higher apparent diffusion coefficient (ADC) values than malignant masses [51]. For example, the ADC values of oncocytomas have been reported to be higher (mean ± SD, $2.0 \pm 0.08 \times 10^{-3}$ mm^2/s) than those of RCC ($1.5 \pm 0.08 \times 10^{-3}$ mm^2/s). However, the low ADCs reported for the general population of RCCs may be primarily driven by the markedly impeded diffusion characteristic of pRCC and the impeded diffusion seen in a small subset of ccRCCs [52–55]. It is common for ADC values in ccRCC to be similar to those of benign masses [54, 55] and higher than those of fat-poor AML [56, 57]. Overall, the use of DWI (and ADC) in the characterization of renal masses suffers from substantial overlap between benign and malignant diseases that limits its usefulness as a single technique [58]. However, DWI may aid in the differentiation of some histologic subtypes, particularly when included in a comprehensive mpMRI assessment (discussed later), and may help in estimating tumor grade. Marked focal intratumoral impeded diffusion increases the likelihood of high-grade ccRCC, with reported sensitivities, specificities, and accuracy of 65–90%, 71–83%, and 83%, respectively [58].

Using these previously reported imaging features, mpMRI-based diagnostic algorithms have been constructed to assist with characterizing renal masses [40, 41, 59, 60]. An algorithm by Kay and Pedrosa [60] has been subsequently tested in both retrospective and prospective analyses [40, 41] (Fig. 4). An algorithm by Cornelis and Grenier [59] contains similar principles, but to our knowledge the accuracy of that algorithm has not been reported. The first step in the algorithm by Kay and Pedrosa [60] assesses the signal intensity on T2-weighted images and determines whether the lesion is hyper-, iso-, or

hypointense relative to renal cortex. Masses are then further subdivided by the degree of enhancement at corticomedullary phase imaging (i.e., timed with MRI-fluoroscopic technique at approximately 40 seconds after contrast material injection) according to previously reported enhancement ratios [37]: intense (greater than or equal to renal cortex), moderate (near 50% of renal cortex), or mild (near 25–30% of renal cortex). Additional features (e.g., presence of microscopic fat, SEI) are then used to favor a particular subtype.

Renal neoplasms hyperintense relative to renal cortex on T2-weighted images include ccRCC, oncocytoma, and chrRCC [60]. If a mass is determined to have intense enhancement, ccRCC and oncocytoma would be the two primary considerations. Of these, the presence of microscopic fat would strongly favor ccRCC. Masses hyperintense relative to renal cortex on T2-weighted images and moderately enhancing would primarily include oncocytoma and chrRCC, with preliminary findings suggesting the former is favored if SEI is present. A substantial overlap exists for renal masses that are isointense to renal cortex on T2-weighted images; both RCC and oncocytoma may have this appearance. Among T2-isointense masses, ccRCC is suspected if the mass is heterogeneous or has microscopic fat, oncocytoma is suspected if SEI is present, chrRCC is suspected if moderately enhancing and homogeneous, and pRCC is suspected if there is mild progressive enhancement. Finally, among masses that are hypointense to renal cortex on T2-weighted images, fat-poor AML, pRCC, and rarely ccRCC are possible. Of these, both fat-poor AML and ccRCC usually show intense enhancement, whereas pRCC usually shows mild progressive enhancement. Impeded diffusion, an arterial-delayed enhancement ratio of greater than 1.5, and homogeneity favor fat-poor AML over ccRCC in this subset of renal masses. A decrease in signal intensity on longer-TE in-phase imaging relative to shorter-TE opposed-phase T1-weighted dual-echo gradient-echo imaging indicates susceptibility artifact and usually is attributed to the presence of iron in malignant tumors such as pRCC and, less commonly, ccRCC [61].

Canvasser et al. [41] evaluated the utility of this mpMRI-based algorithm to produce a Likert score that conveys the likelihood of ccRCC in cT1a renal masses, which they termed the “clear cell likelihood score” or “ccLS,” and defined as follows: 1, very unlikely; 2, unlikely; 3, equivocal; 4, likely; and 5, highly likely. For example, a mass showing hyperintense signal on T2-weighted images, intense enhancement, and microscopic fat would receive a ccLS of 5 (highly likely ccRCC), whereas a mass showing hypointense signal on T2-weighted images and mild progressive enhancement would be designated a ccLS of 1 (very unlikely ccRCC). In that study [41], a ccLS threshold of 4 or greater yielded 79% accuracy, 78% sensitivity, and 80% specificity for ccRCC, and a ccLS threshold of 2 or less yielded 95% specificity and 93% PPV for non-ccRCC neoplasms (benign and malignant). Preliminary prospective data from 125 masses (cT1a–T3) [62] yielded 89.6% accuracy, 92.3% sensitivity, 85.1% specificity, 91.1% PPV, and 87% NPV for ccRCC using a ccLS threshold of 4 or greater and 87.2% accuracy, 68.1% sensitivity, 98.7% specificity, 97% PPV, and 83.7% NPV for non-ccRCC neoplasms using a ccLS threshold of 2 or less.

Technetium-99m-Sestamibi

Technetium-99m-sestamibi is a U. S. Food and Drug Administration–approved radiotracer taken up by cells with a high concentration of mitochondria. It has several uses, including the assessment of coronary artery disease (by identifying myocardial ischemia) and localizing parathyroid adenomas [63, 64]. However, ^{99m}Tc-sestamibi also can be used to differentiate oncocytomas and hybrid oncocytic-chromophobe tumors (HOCTs) from more aggressive renal neoplasms [65–68]. At ^{99m}Tc-sestamibi SPECT/CT, oncocytomas show radiotracer uptake similar to or above uninvolved renal parenchyma, which is hypothesized to be because of densely packed dysfunctional mitochondria [69]. However, the relationship between mitochondrial dysfunction and the degree of radiotracer uptake is not well understood [70].

Tumors derived from proximal renal tubules, such as ccRCC and pRCC, show less ^{99m}Tc-sestamibi uptake than uninvolved renal parenchyma and oncocytic neoplasms. This is believed to be related to the high expression of multidrug resistance pumps that limit the accumulation of ^{99m}Tc-sestamibi [66, 71]. In a prospective trial involving 50 patients with clinical T1 renal masses, ^{99m}Tc-sestamibi SPECT/CT was positive in five of six oncocytomas, two of two HOCTs, two of four chrRCCs, zero of one AML, and zero of 37 ccRCCs or pRCCs, for an overall sensitivity and specificity of 87.5% and 92.5%, respectively [68]. Although unable to differentiate between oncocytoma, HOCT, and chrRCC, the noninvasive diagnosis of an oncocytic neoplasm is clinically valuable because this diagnosis would be typically associated with a benign or indolent tumor. Another smaller study of 27 patients reported similar findings; 11 of 12 oncocytomas, three of three HOCTs, and one of three pRCC showed radiotracer uptake, whereas the 11 remaining RCCs did not [67].

Clinical Implementation of a Multimodal Algorithm for Renal Masses

The ultimate goal of an imaging evaluation of a renal mass is to diagnose benign causes that obviate further testing (including RMB) or surgery, identify masses that might be best suited for AS, and enable treatment of life-threatening cancers. Historically, all solid renal masses without macroscopic fat used to be removed in eligible patients because the risks of RMB were deemed too high and the likelihood of benign disease deemed too low to warrant an alternative strategy. This paradigm resulted in many benign masses and masses of low malignant potential being resected. In recent years, better understanding of the natural history of small renal masses and clearer data indicating the relative safety of RMB have facilitated adoption of RMB before surgery to establish a histologic diagnosis, predict biologic behavior, select patients for AS, and minimize overtreatment. However, there are caveats to the routine use of RMB. A renal mass may be in an unfavorable anatomic location that is more prone to complication (e.g., hilar mass) [72], and not all masses may require RMB (e.g., a mass highly likely to be benign at imaging [e.g., fat-poor AML], a mass highly likely to be malignant at imaging [e.g., ccLS of 5] that will undergo treatment regardless of RMB results). Therefore, RMB has the greatest potential impact in patients in whom the presence of malignancy is uncertain and, more importantly, those in whom AS is being contemplated (i.e., to rule out aggressive forms of RCC). Incorporation of mpMRI into the workup of an indeterminate renal mass could reduce the number of biopsies, expedite

treatment in high-risk patients, minimize complications, and potentially reduce the cost of care.

Multiparametric MRI–based diagnostic algorithms provide a framework for a multimodal clinical approach to renal masses, a method that could incorporate mpMRI, RMB, and ^{99m}Tc-sestarnibi SPECT/CT. Although this approach would require further prospective validation before widespread implementation, there are some compelling use cases that should drive this effort forward. For example, although the decision to treat is ultimately based on multiple factors, patients with a small renal mass receiving a ccLS of 1 or 2 could be offered AS without RMB. Most of these masses are slow-growing, indolent pRCCs [41, 62, 73]. Follow-up imaging in 6 months and annually thereafter can be used to detect growth in the tumor in the rare event in which a tumor with a ccLS of 1 or 2 represents a more aggressive histologic diagnosis. In contrast, definitive treatment without RMB can be offered for masses with a ccLS of 4 or 5 (PPV for ccRCC in cT1a renal masses of ≈ 85%) (Fig. 5). Whether this cohort (and those with a ccLS of 2 or 3 and SEI) would benefit from preoperative ^{99m}Tc-sestamibi SPECT/CT to reduce falsepositive findings related to oncocytic neoplasms needs to be determined in cost-effectiveness studies (Fig. 6).

For cT1a renal masses, RMB may have greatest benefit for those with a ccLS of 3 because approximately half are ccRCC (Fig. 7). Only 20% of cT1a renal masses are ccLS of 3. Restricting biopsy to this group would eliminate 80% of RMBs, result in unnecessary surgery (i.e., unbiopsied tumors with a ccLS of 1, 2, 4, or 5) for oncocytoma and fat-poor AML in 4.5% and 1.7%, respectively, and result in 4% of ccRCCs being placed on AS [41]. The latter should be acceptable given the proven safety of AS for follow-up of small renal masses [74]. Incorporation of ^{99m}Tc-sestamibi SPECT/CT in cases in which oncocytoma is considered on the basis of imaging findings (e.g., SEI) would likely reduce further the number of unnecessary surgeries.

Although mpMRI-based diagnostic algorithms have the greatest potential in incidental small renal masses, it also may play an important role in the management of patients with larger tumors. AS is contemplated in some patients with comorbidities and cT1b–T2 renal masses. Multiparametric MRI may be complementary to RMB in some patients and enable avoidance of RMB in others. Further testing to assess the performance of mpMRI in predicting tumor grade would be particularly important for this latter application. Similarly, mpMRI may help in the management of patients with locally advanced and metastatic disease at presentation in whom selection of various options for systemic therapy or debulking nephrectomy or both are being considered.

Conclusion

Data are accumulating that support a greater role of imaging in managing renal masses that should eliminate the need for percutaneous RMB in many patients. A diagnostic imaging algorithm based largely on mpMRI features that expresses the likelihood of ccRCC shows promise in distinguishing benign from malignant small solid renal masses (and possibly larger tumors as well) and in predicting histologic subtype (so-called “virtual biopsy”). Ultimately, prospective multisite validation and cost-effectiveness studies are required before

widespread implementation. Further research is being conducted that will help clarify the future role of the virtual biopsy in the management of renal masses.

Acknowledgment

We thank Erin Moore for the artistic rendering of the algorithm illustrated in Figure 4.

Supported in part by National Institutes of Health grants R01CA154475 to I. Pedrosa and J. A. Cadeddu, P50CA196516 to I. Pedrosa and J. A. Cadeddu, and U01CA207091 to I. Pedrosa.

References

1. Siegel RL, Miller KD, Jemal A. Cancer statistics, 2018. CA Cancer J Clin 2018; 68:7–30 [PubMed: 29313949]
2. Hollingsworth JM, Miller DC, Daignault S, Hollenbeck BK. Rising incidence of small renal masses: a need to reassess treatment effect. J Natl Cancer Inst 2006; 98:1331–1334 [PubMed: 16985252]
3. Frank I, Blute ML, Cheville JC, Lohse CM, Weaver AL, Zincke H. Solid renal tumors: an analysis of pathological features related to tumor size. J Urol 2003; 170:2217–2220 [PubMed: 14634382]
4. Johnson DC, Vukina J, Smith AB, et al. Preoperatively misclassified, surgically removed benign renal masses: a systematic review of surgical series and United States population level burden estimate. J Urol 2015; 193:30–35 [PubMed: 25072182]
5. Lopez-Beltran A, Carrasco JC, Cheng L, Scarpelli M, Kirkali Z, Montironi R. 2009 Update on the classification of renal epithelial tumors in adults. Int J Urol 2009; 16:432–443 [PubMed: 19453547]
6. Remzi M, Ozsoy M, Klingler HC, et al. Are small renal tumors harmless? Analysis of histopathological features according to tumors 4 cm or less in diameter. J Urol 2006; 176:896–899 [PubMed: 16890647]
7. Thompson RH, Kurta JM, Kaag M, et al. Tumor size is associated with malignant potential in renal cell carcinoma cases. J Urol 2009; 181:2033–2036 [PubMed: 19286217]
8. Duchene DA, Lotan Y, Cadeddu JA, Sagalowsky AI, Koeneman KS. Histopathology of surgically managed renal tumors: analysis of a contemporary series. Urology 2003; 62:827–830 [PubMed: 14624902]
9. Amin MB, Amin MB, Tamboli P, et al. Prognostic impact of histologic subtyping of adult renal epithelial neoplasms: an experience of 405 cases. Am J Surg Pathol 2002; 26:281–291 [PubMed: 11859199]
10. Campbell S, Uzzo RG, Allaf ME, et al. Renal mass and localized renal cancer: AUA guideline. J Urol 2017; 198:520–529 [PubMed: 28479239]
11. Mehrazin R, Smaldone MC, Kutikov A, et al. Growth kinetics and short-term outcomes of cT1b and cT2 renal masses under active surveillance. J Urol 2014; 192:659–664 [PubMed: 24641909]
12. Sanchez A, Feldman AS, Hakimi AA. Current management of small renal masses, including patient selection, renal tumor biopsy, active surveillance, and thermal ablation. J Clin Oncol 2018 Oct 29 [Epub ahead of print]
13. Richard PO, Lavallée LT, Pouliot F, et al. Is routine renal tumor biopsy associated with lower rates of benign histology following nephrectomy for small renal masses? J Urol 2018; 200:731–736 [PubMed: 29653161]
14. Finelli A, Ismaila N, Russo P. Management of small renal masses: American Society of Clinical Oncology Clinical Practice Guideline Summary J Oncol Pract 2017; 13:276–278 [PubMed: 28118108]
15. Motzer RJ, Jonasch E, Agarwal N, et al. Kidney cancer, version 2.2017, NCCN Clinical Practice Guidelines in Oncology. J Natl Compr Canc Netw 2017; 15:804–834 [PubMed: 28596261]
16. Heilbrun ME, Remer EM, Casalino DD, et al. ACR Appropriateness Criteria indeterminate renal mass. J Am Coll Radiol 2015; 12:333–341 [PubMed: 25842014]
17. Marconi L, Dabestani S, Lam TB, et al. Systematic review and meta-analysis of diagnostic accuracy of percutaneous renal tumour biopsy. Eur Urol 2016; 69:660–673 [PubMed: 26323946]

18. Patel HD, Johnson MH, Pierorazio PM, et al. Diagnostic accuracy and risks of biopsy in the diagnosis of a renal mass suspicious for localized renal cell carcinoma: systematic review of the literature. J Urol 2016; 195:1340–1347 [PubMed: 26901507]
19. Salmasi A, Faiena I, Lenis AT, Pooli A, Johnson DC, Drakaki A, et al. Association between renal mass biopsy and upstaging to perinephric fat involvement in a contemporary cohort of patients with clinical T1a renal cell carcinoma. Urol Oncol 2018; 36:527.e13–e19
20. Patel HD, Druskin SC, Rowe SP, Pierorazio PM Gorin MA, Allaf ME. Surgical histopathology for suspected oncocytoma on renal mass biopsy: a systematic review and meta-analysis. BJU Int 2017; 119:661–666 [PubMed: 28058773]
21. Young JR, Margolis D, Sauk S, Pantuck AJ, Sayre J, Raman SS. Clear cell renal cell carcinoma: discrimination from other renal cell carcinoma subtypes and oncocytoma at multiphasic multidetector CT. Radiology 2013; 267:444–453 [PubMed: 23382290]
22. Zhang J, Lefkowitz RA, Ishill NM, et al. Solid renal cortical tumors: differentiation with CT. Radiology 2007; 244:494–504 [PubMed: 17641370]
23. Wang Z, Davenport M, Silverman S, et al. CT renal mass protocols v1.0. c.ymcdn.com/sites/www.abdominalradiology.org/resource/resmgr/education_dfp/RCC/RCC.CTprotocolsfinal-7-15-17.pdf. Published 2018. Accessed January 10, 2019
24. Ruppert-Kohlmayr AJ, Uggowitzer M, Meissnitzer T, Ruppert G. Differentiation of renal clear cell carcinoma and renal papillary carcinoma using quantitative CT enhancement parameters. AJR 2004; 183:1387–1391 [PubMed: 15505308]
25. Herts BR, Coll DM, Novick AC, et al. Enhancement characteristics of papillary renal neoplasms revealed on triphasic helical CT of the kidneys. AJR 2002; 178:367–372 [PubMed: 11804895]
26. Sasaguri K, Takahashi N, Gomez-Cardona D, et al. Small (< 4 cm) renal mass: differentiation of oncocytoma from renal cell carcinoma on biphasic contrast-enhanced CT. AJR 2015; 205:999–1007 [PubMed: 26496547]
27. Kim JI, Cho JY, Moon KC, Lee HJ, Kim SH. Segmental enhancement inversion at biphasic multidetector CT: characteristic finding of small renal oncocytoma. Radiology 2009; 252:441–448 [PubMed: 19508984]
28. Schieda N, McInnes MD, Cao L. Diagnostic accuracy of segmental enhancement inversion for diagnosis of renal oncocytoma at biphasic contrast enhanced CT: systematic review. Eur Radiol 2014; 24:1421–1429 [PubMed: 24663821]
29. Kim SH, Kim CS, Kim MJ, Cho JY, Cho SH. Differentiation of clear cell renal cell carcinoma from other subtypes and fat-poor angiomyolipoma by use of quantitative enhancement measurement during three-phase MDCT. AJR 2016; 206: [web]W21–W28 [PubMed: 26700359]
30. Yang CW, Shen SH, Chang YH, et al. Are there useful CT features to differentiate renal cell carcinoma from lipid-poor renal angiomyolipoma? AJR 2013; 201:1017–1028 [PubMed: 24147472]
31. Hafron J, Fogarty JD, Hoenig DM, Li M, Berkenblit R, Ghavamian R. Imaging characteristics of minimal fat renal angiomyolipoma with histologic correlations. Urology 2005; 66:1155–1159 [PubMed: 16360431]
32. Lubner MG, Stabo N, Abel EJ, Del Rio AM, Pickhardt PJ. CT textural analysis of large primary renal cell carcinomas: pretreatment tumor heterogeneity correlates with histologic findings and clinical outcomes. AJR 2016; 207:96–105 [PubMed: 27145377]
33. Schieda N, Thornhill RE, Al-Subhi M, et al. Diagnosis of sarcomatoid renal cell carcinoma with CT: evaluation by qualitative imaging features and texture analysis. AJR 2015; 204:1013–1023 [PubMed: 25905936]
34. Hodgdon T, McInnes MD, Schieda N, Flood TA, Lamb L, Thornhill RE. Can quantitative CT texture analysis be used to differentiate fat-poor renal angiomyolipoma from renal cell carcinoma on unenhanced CT images? Radiology 2015; 276:787–796 [PubMed: 25906183]
35. Raman SP, Chen Y, Schroeder JL, Huang P, Fishman EK. CT texture analysis of renal masses: pilot study using random forest classification for prediction of pathology. Acad Radiol 2014; 21:1587–1596 [PubMed: 25239842]

36. Feng Z, Rong P, Cao P, et al. Machine learning-based quantitative texture analysis of CT images of small renal masses: differentiation of angiomyolipoma without visible fat from renal cell carcinoma. Eur Radiol 2018; 28:1625–1633 [PubMed: 29134348]
37. Sun MR, Ngo L, Genega EM, et al. Renal cell carcinoma: dynamic contrast-enhanced MR imaging for differentiation of tumor subtypes—correlation with pathologic findings. Radiology 2009; 250:793–802 [PubMed: 19244046]
38. Vargas HA, Chaim J, Lefkowitz RA, et al. Renal cortical tumors: use of multiphasic contrast-enhanced MR imaging to differentiate benign and malignant histologic subtypes. Radiology 2012; 264:779–788 [PubMed: 22829683]
39. Young JR, Coy H, Kim HJ, et al. Performance of relative enhancement on multiphasic MRI for the differentiation of clear cell renal cell carcinoma (RCC) from papillary and chromophobe RCC subtypes and oncocytoma. AJR 2017; 208:812–819 [PubMed: 28125273]
40. Kay FU, Canvasser NE, Xi Y, et al. Diagnostic performance and interreader agreement of a standardized MR imaging approach in the prediction of small renal mass histology. Radiology 2018; 287:543–553 [PubMed: 29390196]
41. Canvasser NE, Kay FU, Xi Y, et al. Diagnostic accuracy of multiparametric magnetic resonance imaging to identify clear cell renal cell carcinoma in cT1a renal masses. J Urol 2017; 198:780–786 [PubMed: 28457802]
42. Pedrosa I, Chou MT, Ngo L, et al. MR classification of renal masses with pathologic correlation. Eur Radiol 2008; 18:365–375 [PubMed: 17899106]
43. Sun MR, Pedrosa I. Magnetic resonance imaging of renal masses. Semin Ultrasound CT MR 2009; 30:326–351 [PubMed: 19711644]
44. Ramamurthy NK, Moosavi B, McInnes MD, Flood TA, Schieda N. Multiparametric MRI of solid renal masses: pearls and pitfalls. Clin Radiol 2015; 70:304–316 [PubMed: 25472466]
45. Earls JP, Rofsky NM, DeCorato DR, Krinsky GA, Weinreb JC. Hepatic arterial-phase dynamic gadolinium-enhanced MR imaging: optimization with a test examination and a power injector. Radiology 1997; 202:268–273 [PubMed: 8988222]
46. Hindman N, Ngo L, Genega EM, et al. Angiomyolipoma with minimal fat: can it be differentiated from clear cell renal cell carcinoma by using standard MR techniques? Radiology 2012; 265:468–477 [PubMed: 23012463]
47. Pedrosa I, Sun MR, Spencer M, et al. MR imaging of renal masses: correlation with findings at surgery and pathologic analysis. RadioGraphics 2008; 28:985–1003 [PubMed: 18635625]
48. Schieda N, Davenport M, Pedrosa I, et al. Renal and adrenal masses containing fat at MRI: proposed nomenclature by the Society of Abdominal Radiology Disease-Focused Panel on Renal Cell Carcinoma. J Magn Reson Imaging 2019 Jan 28 [Epub ahead of print]
49. Rosenkrantz AB, Hindman N, Fitzgerald EF, Niver BE, Melamed J, Babb JS. MRI features of renal oncocytoma and chromophobe renal cell carcinoma. AJR 2010; 195:[web]W421–W427 [PubMed: 21098174]
50. Sasiwimonphan K, Takahashi N, Leibovich BC, Carter RE, Atwell TD, Kawashima A. Small (<4 cm) renal mass: differentiation of angiomyolipoma without visible fat from renal cell carcinoma utilizing MR imaging. Radiology 2012; 263:160–168 [PubMed: 22344404]
51. Lassel EA, Rao R, Schwenke C, Schoenberg SO, Michaely HJ. Diffusion-weighted imaging of focal renal lesions: a meta-analysis. Eur Radiol 2014; 24:241–249 [PubMed: 24337912]
52. Wang H, Cheng L, Zhang X, et al. Renal cell carcinoma: diffusion-weighted MR imaging for subtype differentiation at 3.0 T. Radiology 2010; 257:135–143 [PubMed: 20713607]
53. Goyal A, Sharma R, Bhalla AS, et al. Diffusion-weighted MRI in renal cell carcinoma: a surrogate marker for predicting nuclear grade and histological subtype. Acta Radiol 2012; 53:349–358 [PubMed: 22496427]
54. Choi YA, Kim CK, Park SY, Cho SW, Park BK. Subtype differentiation of renal cell carcinoma using diffusion-weighted and blood oxygenation level-dependent MRI. AJR 2014; 203: [web]W78–W84 [PubMed: 24951231]
55. Taouli B, Thakur RK, Mannelli L, et al. Renal lesions: characterization with diffusion-weighted imaging versus contrast-enhanced MR imaging. Radiology 2009; 251:398–407 [PubMed: 19276322]

56. Li H, Li A, Zhu H, et al. Whole-tumor quantitative apparent diffusion coefficient histogram and texture analysis to differentiation of minimal fat angiomyolipoma from clear cell renal cell carcinoma. Acad Radiol 2018 Aug 4 [Epub ahead of print]
57. Li H, Liang L, Li A, et al. Monoexponential, biexponential, and stretched exponential diffusion-weighted imaging models: quantitative biomarkers for differentiating renal clear cell carcinoma and minimal fat angiomyolipoma. J Magn Reson Imaging 2017; 46:240–247 [PubMed: 27859853]
58. Kang SK, Zhang A, Pandharipande PV, Chandarana H, Braithwaite RS, Littenberg B. DWI for renal mass characterization: systematic review and meta-analysis of diagnostic test performance. AJR 2015; 205:317–324 [PubMed: 26204281]
59. Cornells F, Grenier N. Multiparametric magnetic resonance imaging of solid renal tumors: a practical algorithm. Semin Ultrasound CT MR 2017; 38:47–58 [PubMed: 28237280]
60. Kay FU, Pedrosa I. Imaging of solid renal masses. Urol Clin North Am 2018; 45:311–330 [PubMed: 30031457]
61. Childs DD, Clingan MJ, Zagoria RJ, et al. In-phase signal intensity loss in solid renal masses on dual-echo gradient-echo MRI: association with malignancy and pathologic classification. AJR 2014; 203: [web]W421–W428 [PubMed: 25247971]
62. Johnson B, Steinberg RL, Pedrosa I, Cadeddu JA. Multiparametric magnetic resonance imaging identifies clear cell renal cell carcinoma with greater accuracy in higher stage lesions, (abstract) In: Scientific Program of 36th World Congress of Endourology program book. www.liebertpub.com/doi/pdfplus/10.1089/end.2018.29043.abstracts. Published 2018. Accessed January 2019
63. Billy HT, Rimkus DR, Hartzman S, Latimer RG. Technetium-99m-sestamibi single agent localization versus high resolution ultrasonography for the preoperative localization of parathyroid glands in patients with primary hyperparathyroidism. Am Surg 1995; 61:882–888 [PubMed: 7668462]
64. Mariani G, Gulec SA, Rubello D, et al. Preoperative localization and radioguided parathyroid surgery. J Nucl Med 2003; 44:1443–1458 [PubMed: 12960191]
65. Gormley TS, Van Every MJ, Moreno AJ. Renal oncocytoma: preoperative diagnosis using technetium 99m sestamibi imaging. Urology 1996; 48:33–39
66. Rowe SP, Gorin MA, Gordetsky J, et al. Initial experience using ^{99m}Tc-MIBI SPECT/CT for the differentiation of oncocytoma from renal cell carcinoma. Clin Nucl Med 2015; 40:309–313 [PubMed: 25608174]
67. Tzortzakakis A, Gustafsson O, Karlsson M, Ekström-Ehn L, Ghaffarpour R, Axelsson R. Visual evaluation and differentiation of renal oncocytomas from renal cell carcinomas by means of ^{99m}Tc-sestamibi SPECT/CT. EJNMMI Res 2017; 7:29 [PubMed: 28357787]
68. Gorin MA, Rowe SP, Baras AS, et al. Prospective evaluation of (99m)Tc-sestamibi SPECT/CT for the diagnosis of renal oncocytomas and hybrid oncocytic/chromophobe tumors. Eur Urol 2016; 69:413–416 [PubMed: 26386607]
69. Tickoo SK, Lee MW, Eble JN, et al. Ultrastructural observations on mitochondria and microvesicles in renal oncocytoma, chromophobe renal cell carcinoma, and eosinophilic variant of conventional (clear cell) renal cell carcinoma. Am J Surg Pathol 2000; 24:1247–1256 [PubMed: 10976699]
70. Joshi S, Tolkunov D, Aviv H, et al. The genomic landscape of renal oncocytoma identifies a metabolic barrier to tumorigenesis. Cell Reports 2015; 13:1895–1908 [PubMed: 26655904]
71. Hendrikse NH, Franssen EJ, van der Graaf WT, et al. ^{99m}Tc-sestamibi is a substrate for P-glycoprotein and the multidrug resistance-associated protein. Br J Cancer 1998; 77:353–358 [PubMed: 9472628]
72. Cooper S, Flood TA, Khodary ME, et al. Diagnostic yield and complication rate in percutaneous needle biopsy of renal hilar masses with comparison with renal cortical mass biopsies in a cohort of 195 patients. AJR 2019 Jan 19 [Epub ahead of print]
73. Dodelzon K, Mussi TC, Babb JS, Taneja SS, Rosenkrantz AB. Prediction of growth rate of solid renal masses: utility of MR imaging features—preliminary experience. Radiology 2012; 262:884–893 [PubMed: 22267588]

74. McIntosh AG, Ristau BT, Ruth K, et al. Active surveillance for localized renal masses: tumor growth, delayed intervention rates, and >5-yr clinical outcomes. Eur Urol 2018; 74:157–164 [PubMed: 29625756]

75. Kay FU, Pedrosa I. Imaging of solid renal masses. Radiol Clin North Am 2017; 55:243–258 [PubMed: 28126214]

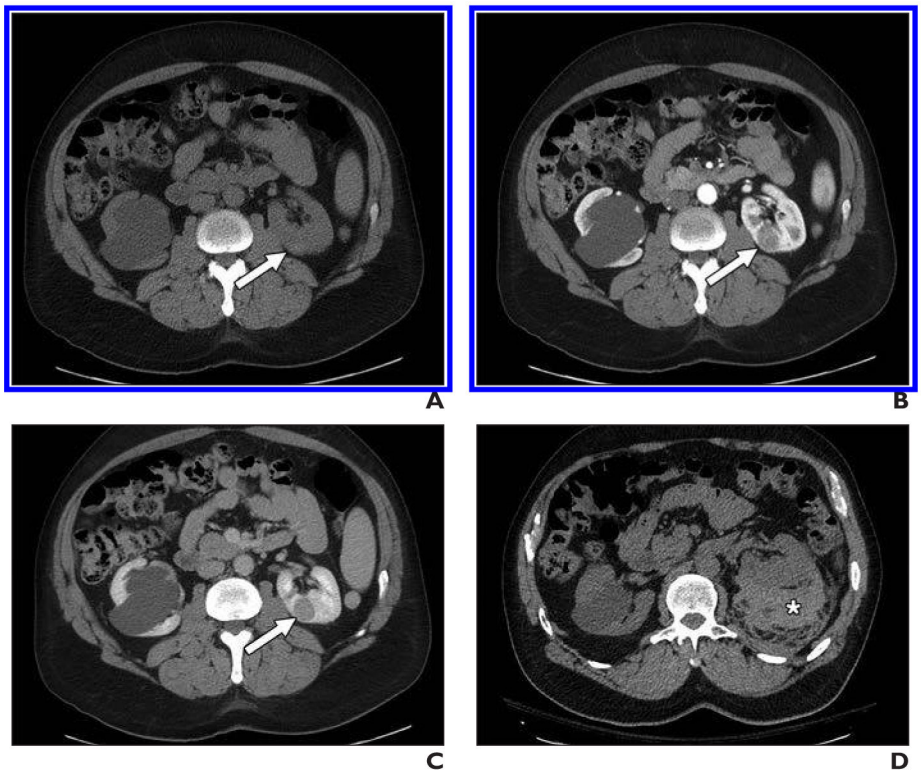

Fig. 1. 56-year-old man with left renal mass.

A–C, Unenhanced axial CT image (**A**) and contrast-enhanced axial CT images acquired during corticomedullary (**B**) and nephrographic (**C**) phases show homogeneous and progressively enhancing mass in posterior medial left kidney (*arrow*), which is mildly hyperattenuating on unenhanced image. Mass was favored to represent papillary renal cell carcinoma (pRCC), and patient underwent percutaneous renal mass biopsy.

D, Postbiopsy CT was performed because patient reported pain. Representative unenhanced CT image shows moderate perinephric hematoma along posterior left kidney (*asterisk*). Patient was admitted to hospital and observed; no transfusion or other support other than observation was reguired. Biopsy confirmed diagnosis of pRCC. After partial nephrectomy, final diagnosis of type I pRCC was rendered.

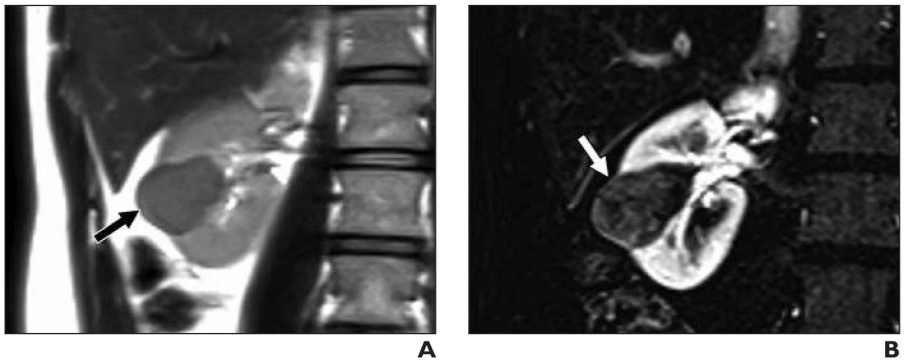

Fig. 2. 43-year-old woman with 3.5-cm right renal mass.

A, Coronal T2-weighted single-shot fast spin-echo image shows mass arising from lower pole of right kidney (*arrow*), which appears hypointense relative to renal cortex.

B, Subtraction of fat-saturated T1-weighted gradient-echo coronal image acquired during corticomedullary phase minus unenhanced acquisition with same parameters shows low-level enhancement within renal mass (*arrow*). This lesion received clear cell likelihood score of 1. Patient subsequently underwent partial nephrectomy and was found to have papillary renal cell carcinoma, International Society of Urological Pathology grade 2.

Fig. 3. 42-year-old woman with 2.1-cm right renal mass.

A, Coronal T2-weighted single-shot fast spin-echo image shows right upper renal mass (*arrow*), which appears hypointense relative to renal cortex.

B and **C,** On coronal fat-saturated T1-weighted gradient-echo images acquired during corticomedullary (**B**) and late nephrographic (**C**) phases, lesion (*arrow*) shows intense enhancement and washout, respectively. Lesion was assigned clear cell likelihood score of 2. Because of location of lesion, safe path for percutaneous renal mass biopsy could not be identified. Patient underwent partial nephrectomy; histopathology results and positive homatropine methylbromide 45 immunostaining confirmed angiomyolipoma.

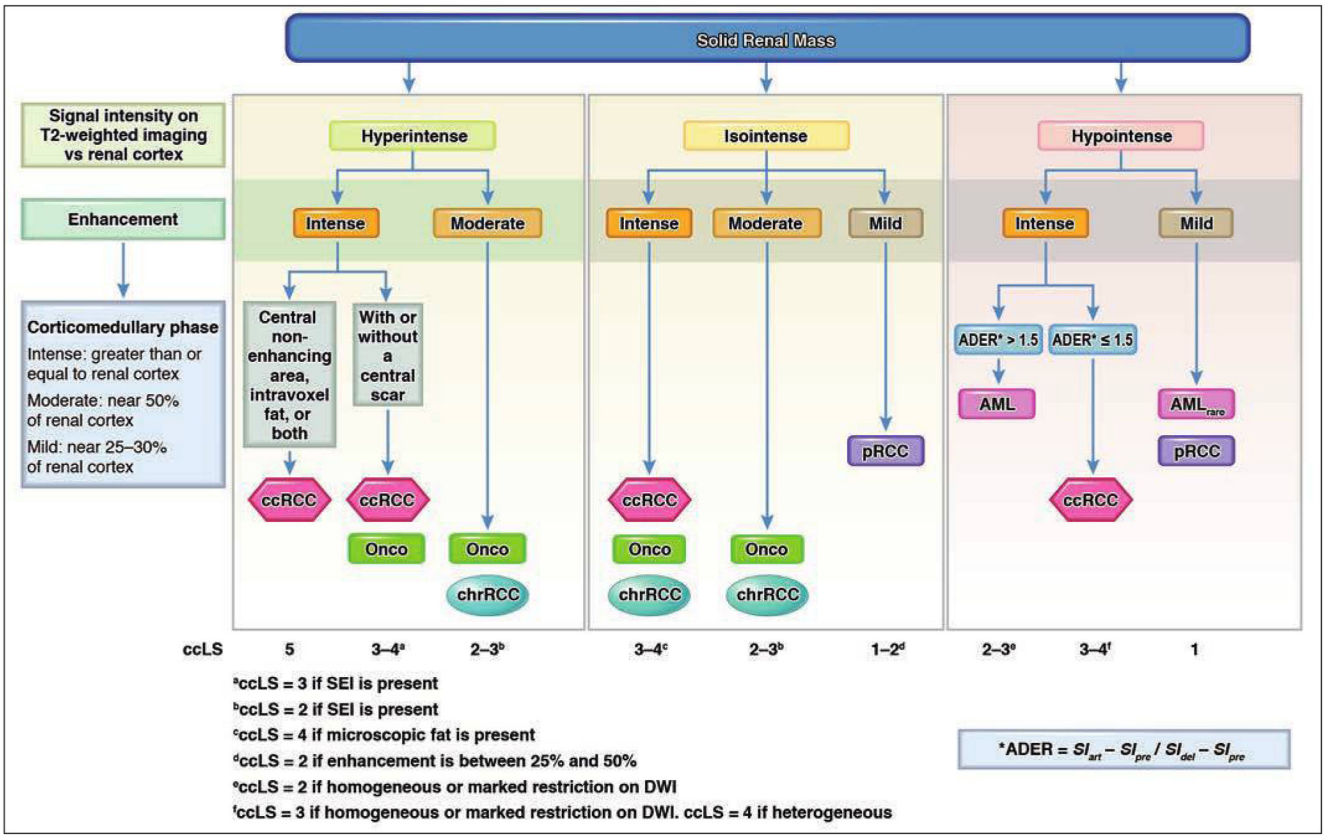

Fig. 4.

Flowchart shows algorithm for characterization of solid renal masses by using imaging features on MRI and assigning clear cell likelihood score (ccLS); ccLS is Likert score that conveys likelihood of clear cell renal cell carcinoma (ccRCC) and is defined as follows: 1, very unlikely; 2, unlikely; 3, equivocal; 4, likely; and 5, highly likely. First step in algorithm is to assess signal intensity of renal mass on T2-weighted images and determine whether mass is hyper-, iso-, or hypointense relative to renal cortex. Masses are then subdivided by degree of enhancement during corticomedullary phase imaging: intense, moderate, or mild. Additional features (e.g., presence of microscopic fat, segmental enhancement inversion [SEI], appearance on DWI) are then used to ultimately assign ccLS value. ADER = arterial-delayed enhancement ratio, AML = angiomyolipoma, AML_{rare} = angiomyolipoma (rare presentation), pRCC = papillary renal cell carcinoma, Onco = oncocytoma, chrRCC = chromophobe renal cell carcinoma, SI_{art} = signal intensity on arterial phase images, SI_{pre} = signal intensity on unenhanced images, SI_{del} = signal intensity on delayed phase images (illustration by Moore E). (Adapted from [75] *Radiologic Clinics of North America,* Vol. 55, Kay FU, Pedrosa I. “Imaging of Solid Renal Masses,” Pages 243–258, Copyright 2018 with permission from Elsevier)

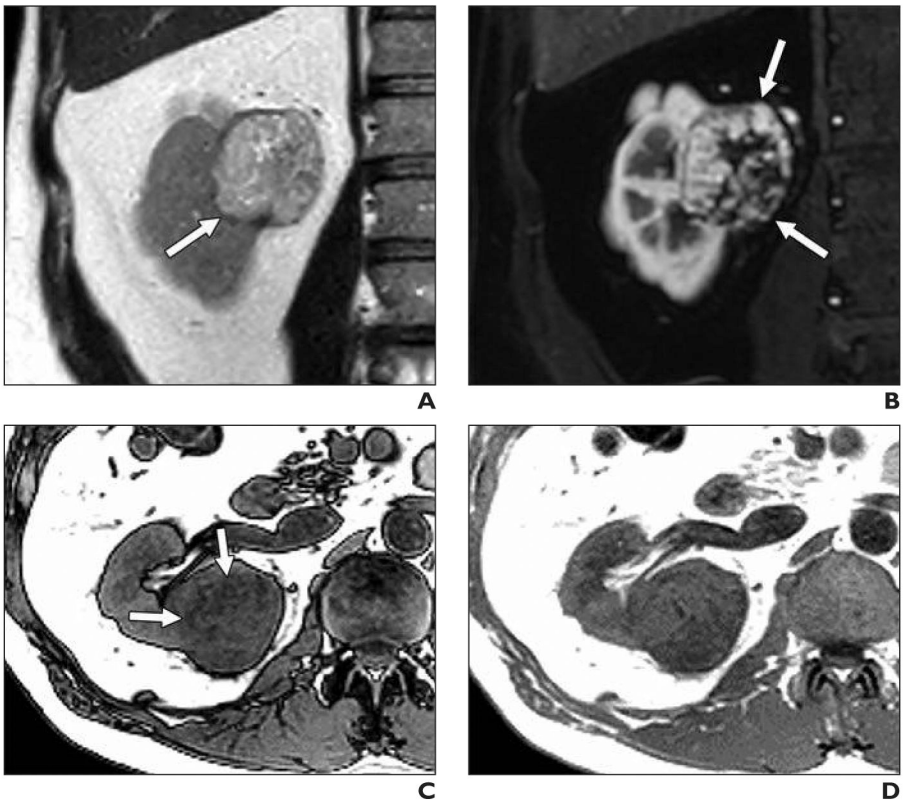

Fig. 5. 47-year-old man with renal mass.

A, Coronal T2-weighted single-shot fast spin-echo image shows mass in medial right kidney (*arrow*) that is heterogeneously hyperintense relative to renal cortex.

B, On coronal fat-saturated T1-weighted gradient-echo image acquired during corticomedullary phase, lesion (*arrows*) shows intense heterogeneous enhancement.

C and **D,** Region of decreased signal intensity (*arrows*, **C**) is present on axial opposed-phased gradient-echo T1-weighted image compared with in-phase gradient-echo image (**D**); this finding is consistent with microscopic fat within tumor. This lesion was given clear cell likelihood score of 5. Patient underwent partial nephrectomy, and histopathology showed clear cell renal cell carcinoma, International Society of Urological Pathology grade 3.

Fig. 6. 57-year-old man with 3.7-cm solid right renal mass.

A, Coronal T2-weighted image shows mildly heterogeneous mass (*arrow*) centered in upper pole of right kidney that is predominantly isointense to renal cortex with slightly hyperintense central region.

B, T1-weighted gradient-echo image acquired during corticomedullary phase shows two distinct patterns of enhancement in mass: region of intense enhancement peripherally (*white arrow*) and central area of hypoenhancement (*black arrow*).

C, T1-weighted gradient-echo image acquired during nephrographic phase shows inversion of signal intensities. Central area now shows hyperintense signal (*black arrow*) relative to remainder of mass, which now appears hypointense (*white arrow*). This enhancement pattern is consistent with presence of segmental enhancement inversion. This mass should receive clear cell likelihood score of 3. Given size of mass, patient underwent renal mass biopsy before being placed on active surveillance; histopathology revealed oncocytoma.

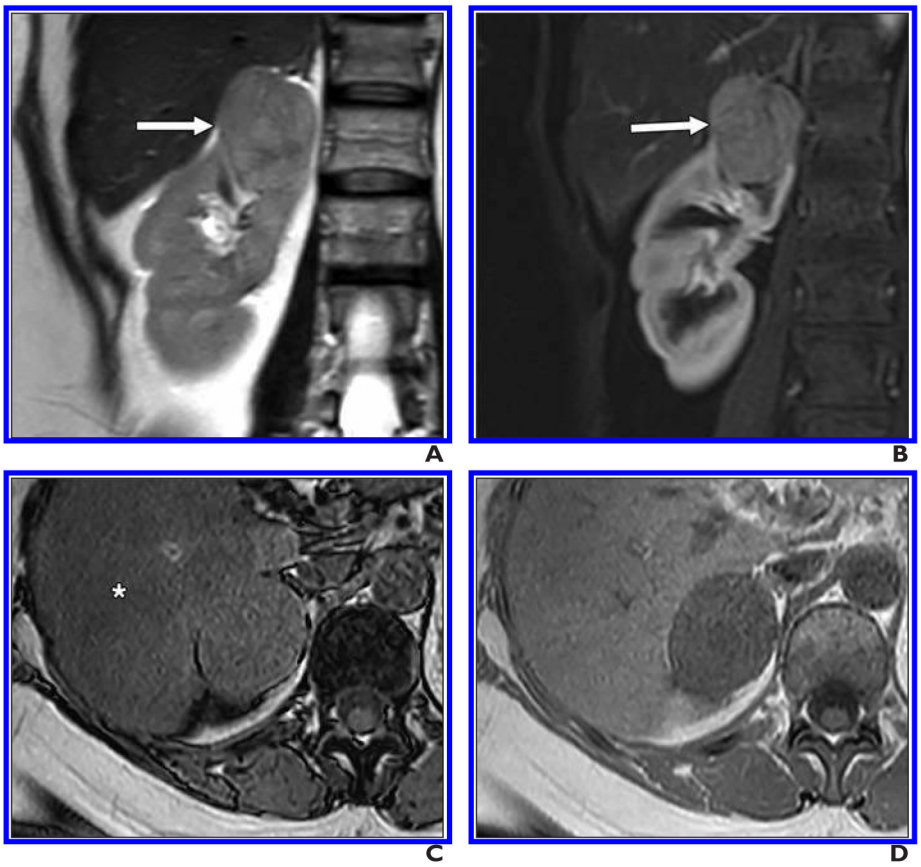

Fig. 7. 44-year-old man with solid right renal mass.

A, Coronal T2-weighted single-shot fast spin-echo image shows mildly heterogeneous mass (*arrow*) is isointense to renal cortex and arising from upper pole of right kidney.

B, Coronal fat-saturated T1-weighted gradient-echo image acquired during corticomedullary phase shows moderate enhancement in mass (*arrow*).

C and **D,** Axial opposed-phase (**C**) and in-phase (**D**) gradient-echo T1-weighted images show no intralesional fat. Incidentally, decreased signal intensity (*asterisk*, **C**) in liver consistent with hepatic steatosis is noted on opposed-phase imaging. This lesion was given clear cell likelihood score of 3. Patient underwent percutaneous renal mass biopsy, and histopathology revealed chromophobe renal cell carcinoma.